





# First-principles self-consistent phonon approach to the study of the vibrational properties and structural phase transition of BaTiO<sub>3</sub>

S. Ehsan , M. Arrigoni , G. K. H. Madsen , and P. Blaha 

*Institute of Materials Chemistry, Vienna University of Technology, Getreidemarkt 9/165-TC, A-1060 Vienna, Austria*

A. Tröster

*Faculty of Physics, University of Vienna, Boltzmannngasse 5, A-1090 Vienna, Austria*



(Received 12 October 2020; accepted 9 March 2021; published 17 March 2021)

We investigate the cubic-to-tetragonal ferroelectric phase transition temperature  $T_c$  of BaTiO<sub>3</sub> through a first-principles self-consistent phonon scheme. This method extends the harmonic approximation by incorporating anharmonic effects due to thermalized displacements, which are simultaneous excitations of phonons with a temperature-dependent random amplitude. The calculated forces are analyzed with an effective harmonic force constant model, which serves as the basis for a new set of thermalized displacements until self-consistency has been reached. The phonons with imaginary frequencies at  $T = 0$  K are stabilized due to anharmonic effects in the temperature range where the corresponding phase is stable and the dynamical instabilities disappear. Using the calculated free energies at various temperatures, volumes, and  $c/a$  ratios, we obtain a thermal expansion in good agreement with the experimental values. Comparing the free energies of the tetragonal and cubic phases at different temperatures, we predict  $T_c \approx 455$  K. This is in reasonable agreement with the experimental value of  $\approx 393$  K in view of the strong influence of the particular density functional theory approximation on the unstable phonon modes.

DOI: [10.1103/PhysRevB.103.094108](https://doi.org/10.1103/PhysRevB.103.094108)

## I. INTRODUCTION

The family of perovskite oxides comprises a wide range of compounds with the general  $ABO_3$  formula unit. These compounds generally undergo multiple phase transitions, which have been extensively studied and characterized along a wide range of temperatures and pressures [1–4]. The study of phase transitions in perovskite oxides is relevant for technological applications, as different phases show a wide range of ferroelectric and piezoelectric properties and electro-optical effects which are widely exploited in technologically important devices [5–8]. Moreover, as the Earth's lower mantle is allegedly mostly composed of the MgSiO<sub>3</sub> perovskite [9], studying the phase transitions of these materials is also relevant for geophysics.

With the advent of increased computational power, *ab initio* calculations based on density functional theory (DFT) are widely performed to interpret experimental results and to predict new materials with desired physical properties. Lattice vibrations play a vital role in different thermodynamical and transport properties, including the study of phase transition at finite temperature and the prediction of lattice thermal conductivity.

In the case of lattice vibrations, the harmonic approximation (HA) is commonly applied and is often adequate for obtaining phonon spectra in agreement with experiments and to examine phase stability. However, the approximation completely breaks down for most of the high-temperature phases of perovskites [10–12] due to dynamical instabilities giving

rise to imaginary phonon frequencies. To overcome this limitation of the HA, several studies have applied a self-consistent phonon (SCP) approach [13–15] to take anharmonic effects in perovskites into account [16–19].

As in other perovskites [11,20–24], BaTiO<sub>3</sub> undergoes a series of phase transitions described by the sequence cubic  $\rightarrow$  tetragonal  $\rightarrow$  orthorhombic  $\rightarrow$  rhombohedral [25–29] as the temperature is decreased. The SCP discussion of such phase transitions mainly concerns the phonon band structure at finite temperature [19]. In this work we show that the high-temperature cubic and tetragonal phases of BaTiO<sub>3</sub> are two examples where the simple HA breaks down. By treating the lattice dynamics using a SCP approach we obtain the finite-temperature phonon spectra of the cubic and tetragonal phases of BaTiO<sub>3</sub> in their stable temperature range without imaginary frequencies. We demonstrate how a very good prediction of unit-cell volume can be obtained and describe how different properties of the material, like lattice parameters, bulk modulus,  $c/a$  ratio, and vibrational free energy, behave as a function of temperature.

The phase transition is studied taking the effect of the temperature dependence of the lattice constants by employing the quasiharmonic approximation (QHA) into account [30]. We discuss our results in the context of earlier phase-transition studies where a strong dependence on volume and DFT functional were demonstrated. We show that a critical temperature  $T_c$  of the cubic-to-tetragonal phase transition in good agreement with the available experimental data is obtained. Finally, we compare our results to effective Hamiltonian simulations

of the phase transition in BaTiO<sub>3</sub> and an SCP study of a similar phase transition in SrTiO<sub>3</sub> which included fourth-order interatomic force constants (IFCs) but neglected thermal expansion [18].

## II. SELF-CONSISTENT PHONON THEORY

At equilibrium the crystal is considered to be in a stable stationary state, in which the crystal potential  $V$  is at a minimum with respect to the equilibrium positions of all atoms in the system. Displacing an atom from its equilibrium position induces forces on all atoms in the system. At any order, these forces can be computed from a suitably truncated Taylor expansion of  $V$ . In particular, in the HA the force experienced by atom  $i$  along the Cartesian direction  $\alpha_1$  due to displacements  $u_{\alpha_2}^j$  of the atoms is given by [31]

$$\begin{aligned} F_{\alpha_1}^i &= - \sum_{j, \alpha_2} \frac{\partial^2 V}{\partial u_{\alpha_1}^i \partial u_{\alpha_2}^j} u_{\alpha_2}^j \\ &= - \sum_{j, \alpha_2} \phi_{\alpha_1 \alpha_2}^{ij} u_{\alpha_2}^j, \end{aligned} \quad (1)$$

where  $\phi_{\alpha_1 \alpha_2}^{ij}$  are the second-order IFCs. Equation (1) shows that it is possible to fit the second-order IFCs to a collection of calculated forces for various configurations of atomic displacements (finite-displacement approach). In general, the use of crystal symmetry can noticeably reduce the number of required displacement configurations, and multiple codes are able to extract IFCs from a modest number of symmetry-independent atomic configurations obtained by slightly displacing a single atom from its equilibrium position [32–34].

Once the second-order IFCs have been obtained, the IFC matrix can be Fourier transformed and diagonalized. This yields phonon frequencies  $\omega(\mathbf{q}s)$  for each mode  $s$  and wave vector  $\mathbf{q}$ , describing the phonon dispersion relation, from which the vibrational free energy and other physical properties can be obtained. However, the analysis of a solid material using the harmonic approximation breaks down if imaginary frequencies are found, which requires taking anharmonic effects into account. To achieve this goal, multiple *ab initio* methods have been proposed. The SCP approach [35] we used in this study is analogous to the one proposed in Refs. [36,37]. It aims at obtaining temperature-dependent IFCs by sampling the crystal potential through the use of the mean-square-displacement (MSD) matrix which describes the mean-square atomic displacements in the system at the desired temperature [38]. The element of the MSD matrix corresponding to atom  $i$  with respect to direction  $\alpha_1$  and to atom  $j$  with respect to direction  $\alpha_2$  is given by

$$\begin{aligned} \Sigma_{\alpha_1 \alpha_2}^{ij} &\equiv \langle u_{\alpha_1}^i u_{\alpha_2}^j \rangle \\ &= \frac{1}{N \sqrt{m_i m_j}} \sum_{\mathbf{q}s} \frac{\langle E(\mathbf{q}s) \rangle}{\omega^2(\mathbf{q}s)} e_{\alpha_1}^i(\mathbf{q}s) e_{\alpha_2}^{j*}(\mathbf{q}s), \end{aligned} \quad (2)$$

where  $N$  is the number of  $\mathbf{q}$  points in the first Brillouin zone,  $m_i$  is the mass of atom  $i$ , and  $\omega(\mathbf{q}s)$  and  $e(\mathbf{q}s)$  are the frequency and the polarization vector of mode  $s$  at point  $\mathbf{q}$  in the Brillouin

zone, respectively.  $\langle E(\mathbf{q}s) \rangle$  is the average energy contribution,

$$\langle E(\mathbf{q}s) \rangle = \hbar \omega(\mathbf{q}s) \left( \langle n(\mathbf{q}s) \rangle + \frac{1}{2} \right),$$

of mode  $\mathbf{q}s$  when the system is in thermal equilibrium at temperature  $T$ , where

$$\langle n(\mathbf{q}s) \rangle = \frac{1}{e^{\hbar \omega(\mathbf{q}s)/k_B T} - 1}$$

represents the average occupation number of phonons in the  $\mathbf{q}s$  mode, as given by the Bose-Einstein distribution. In thermal equilibrium, the MSD matrix acts as the covariance matrix for a multivariate Gaussian distribution

$$p(\mathbf{u}) = \frac{1}{\sqrt{(2\pi)^{3n} |\Sigma|}} e^{-\frac{1}{2} \mathbf{u}^T \Sigma^{-1} \mathbf{u}}, \quad (3)$$

describing the probability density function for the atomic displacements at temperature  $T$ , where  $n$  is the number of atoms in the system and  $\mathbf{u}$  is the  $3n$ -dimensional vector collecting all atomic displacements. In the rest of the study we denote as “thermalized displacements” the atomic displacements sampled using Eq. (3) and as “nonthermalized displacements” the ones obtained from the usual sequential displacements of single atoms.

In our approach, we first calculate volume-dependent IFCs through the use of nonthermalized displacements at different volumes. From these volume-dependent but nonthermalized force constants we get phonons at  $T = 0$  K, which may also include phonons with imaginary frequencies. Then for each volume, the MSD matrix  $\Sigma$  is calculated using a selected temperature and Eq. (2). Afterwards, we draw random samples from the probability distribution  $p(\mathbf{u})$  from which we obtain a new set of thermalized displacements. Then, new thermalized IFCs, phonon eigenvectors, and eigenvalues are obtained. The thermalized IFCs and derived quantities depend on the thermalized displacements, which in turn depend on the IFCs. Therefore, the procedure has to be repeated until a self-consistent solution has been found. With these thermalized IFCs, phonon frequencies which are all stable in the proper temperature range and free energies (see below) are calculated.

## III. SIMULATION DETAILS

### A. Structures

At high temperatures, BaTiO<sub>3</sub> crystallizes into a cubic structure with the  $Pm\bar{3}m$  space group. The unit cell contains five atoms [39], Ba has the Wyckoff position 1a (0, 0, 0), Ti has the position 1b (0.5, 0.5, 0.5), and O has the position 3c (0, 0.5, 0.5). As the temperature decreases, BaTiO<sub>3</sub> undergoes a series of three ferroelectric phase transitions [40]. Around 393 K, it transforms into a tetragonal structure with  $P4mm$  symmetry [27] which is stable until approximately 278 K [41]. Below 278 K it transforms into an orthorhombic phase with  $Pmm2$  symmetry. The rhombohedral low-temperature phase of BaTiO<sub>3</sub> is stable below 183 K [42].

The aim of this paper is to study the cubic  $\rightarrow$  tetragonal transition, which occurs due to the spontaneous polarization along the (001) direction. As a result the tetragonal ( $P4mm$ ) unit cell hosts the same number of atoms as in the cubic structure with four nonequivalent sites: Ba sits at 1a (0, 0, 0),

Ti sits at  $1b(0.5, 0.5, 0.5 + \delta_{\text{Ti}})$ , one symmetry-inequivalent oxygen, O1, is at  $1b(0.5, 0.5, 0.0 + \delta_{\text{O1}})$ , and the other oxygen, O2, is at  $2c(0.5, 0, 0.5 + \delta_{\text{O2}})$ , where  $\delta_{\text{atom}}$  is a free parameter describing the distortion.

### B. Computational details

The *ab initio* DFT calculations in this study were performed using the WIEN2K code [43,44], which employs the (linearized) augmented plane-wave and local orbitals method to solve the Kohn-Sham equations [45]. Details of this method are described in Ref. [44].

Since the energy gain due to the phase transition is small, particular care in the choice of the parameters of the calculations was taken in order to converge the total energy and forces properly. We found that a  $10 \times 10 \times 10$  reciprocal-space  $k$  mesh is sufficient for both types of unit cells. Also of crucial importance is the size of the basis set, which is controlled by the product of the smallest atomic sphere radius  $R_{\text{MT}}^{\text{min}}$  and the plane-wave cutoff  $K_{\text{max}}$ . The calculations of the present work were done with  $R_{\text{MT}}^{\text{min}}K_{\text{max}} = 8.5$  and atomic sphere radii of 2.25, 1.6, and 1.5 bohrs for Ba, Ti, and O, respectively. The energy separation between core and valence states used was  $-6.0$  Ry. Inside the sphere, the maximum angular momentum used in the spherical expansions was  $\ell_{\text{max}} = 10$ , while the charge density in the interstitial was Fourier expanded up to a cutoff of  $G_{\text{max}} = 14$  (*bohr*) $^{-1}$ . We employed the PBEsol exchange-correlation functional [46], which has been devised for obtaining better equilibrium properties of solids, while the local density approximation (LDA) or the generalized gradient approximation of Perdew, Burke, and Ernzerhof (PBE) [47] would lead to much smaller or larger lattice parameters. PBEsol works very well for the prediction of equilibrium volume and harmonic phonon spectra of perovskites [11,23,48,49].

Second-order IFCs were obtained using a  $3 \times 3 \times 3$  supercell expansion containing 135 atoms with a  $2 \times 2 \times 2$  reciprocal  $k$  mesh. Convergence has been checked for a few cases using  $2 \times 2 \times 2$  and  $4 \times 4 \times 4$  supercells and also a denser  $k$  mesh. While some phonon frequencies change by up to  $10$   $\text{cm}^{-1}$  when going from  $2 \times 2 \times 2$  to  $3 \times 3 \times 3$ , these changes are less than  $1$   $\text{cm}^{-1}$  between  $3 \times 3 \times 3$  and  $4 \times 4 \times 4$  supercells. A denser  $k$  mesh changes frequencies by an even smaller amount. Nonthermalized displacements were obtained by displacing atoms in the supercell from their equilibrium positions by  $0.01$  Å. In order to calculate temperature-dependent IFCs, we took for each iteration 30 samples of displacements  $\mathbf{u}$  from the distribution defined by Eq. (3). Self-consistency of the IFCs is typically obtained after 15–20 iterations.

## IV. RESULTS AND DISCUSSION

### A. Structural properties

To calculate equilibrium structural properties like lattice constants  $a$  and  $c$  and bulk moduli  $B$ , we determined the unit-cell dimensions at vanishing hydrostatic pressure. For the cubic phase, this merely amounts to calculating the total energy as a function of the cubic unit-cell volume and fitting

TABLE I. Structural properties of the cubic and tetragonal phases of BaTiO<sub>3</sub> calculated with the PBEsol functional.

	Present work		Other works		
	0 K	475 K	Theory	Expt.	
Cubic			0 K	413 K	473 K
$a$ (Å)	3.972	3.993	3.977 [51]	4.011 [52]	4.013 [52]
$V$ (Å <sup>3</sup> )	62.67	63.67	62.90 [51]	64.53 [52]	64.63 [52]
$B$ (GPa)	179	166	179 [51]	162 [53]	
	Present work		Other works		
			Theory	Expt.	
Tetragonal	0 K	400 K	0 K	398 K	293 K
$a$ (Å)	3.958	3.976	3.962 [51]	4.002 [52]	
$c$ (Å)	4.045	4.052	4.059 [51]	4.028 [52]	
$V$ (Å <sup>3</sup> )	63.37	64.06	63.72 [51]	64.51 [52]	
$c/a$	1.022	1.019 (1.033 <sup>a</sup> )	1.025 [51]	1.007 [52]	
$B$ (GPa)	128	124	148 [51]		134 <sup>b</sup> [54]

<sup>a</sup> $c/a$  obtained at the 400 K volume without taking vibrational contributions to the free energy into account.

<sup>b</sup>Extrapolated at 0 GPa from values in Ref. [54].

the energy values with a Birch-Murnaghan equation of state [50].

The top part of Table I shows the results of our calculations for the cubic phase and reports the equilibrium lattice constant  $a$  and the bulk modulus  $B$ . For comparison, experimental values as well as previous DFT results are also shown. As expected, PBEsol (at 0 K) predicts a value  $a$  for the cubic lattice constant in good agreement with experiments with a discrepancy of around 1% with respect to the experimental result at 413 K. This difference is further reduced to merely 0.5% at 473 K if thermal expansion is taken into account. Similarly, the bulk modulus  $B$  reduces its value from 179 GPa at 0 K to 166 GPa at 475 K, which agrees well with the experimental value of 162 GPa.

Figure 1 shows how the calculated lattice parameter of the cubic phase evolves with temperature and also its comparison

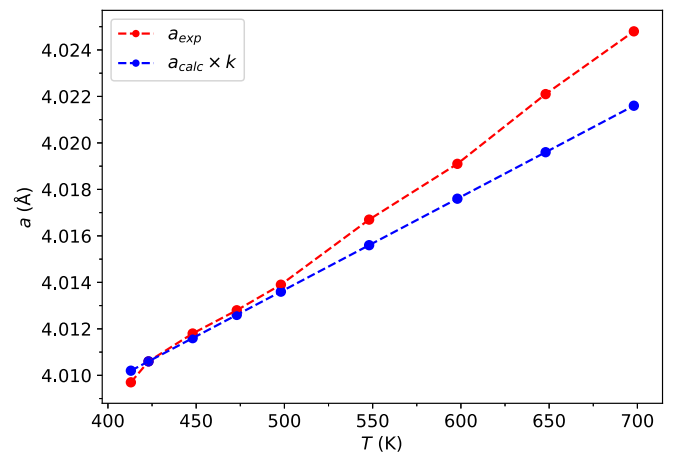


FIG. 1. Temperature dependency of the experimental [52] ( $a_{\text{exp}}$ ) and calculated ( $a_{\text{calc}}(T=423 \text{ K})$ ) lattice constant values in the cubic phase of BaTiO<sub>3</sub>. Here  $k = \frac{a_{\text{exp}}}{a_{\text{calc}}}$ .

with experimental values, where the theoretical values have been shifted to match experiment results at 423 K. In both cases, the lattice parameter increases linearly with temperature, but with different slopes. For the calculated case, the slope is slightly lower than the experimental one, indicating that PBEsol predicts a slightly smaller thermal expansion coefficient  $\alpha = 9.85 \times 10^{-6} \text{ K}^{-1}$ .

The calculations in the tetragonal phase are somewhat more involved since for each unit cell volume, the ratio  $c/a$  between the unit-cell parameters and the free parameters  $\delta$  have to be optimized. We start with the optimization of  $c/a$  at 0 K. We find that the value of  $c/a$  increases with an increase in volume, which agrees with a previous DFT study [48]. This behavior is opposite what is found in other perovskites like SrTiO<sub>3</sub> and RbCaF<sub>3</sub> [11], where  $c/a$  decreases with an increase in volume. Furthermore, it is in disagreement with the experimentally observed decrease of  $c/a$  with increasing temperature. This discrepancy is due to thermal effects beyond expansion and is further discussed in Sec. IV D.

The results for the tetragonal structure are shown in the bottom part of Table I and are compared with the experimental results. As expected, while the theoretical unit-cell volume obtained from our calculations at 0 K is lower than the experimental values, after addition of the vibrational free energy  $F_{\text{vib}}$  and the inclusion of thermal expansion, the resulting equilibrium unit-cell volume is in good agreement with experiment.

### B. Born effective charge and dielectric tensor

To quantitatively understand the splitting between transverse and longitudinal optical phonon modes, we calculated the Born effective charge tensor  $Z^*$  [55] and the dielectric tensor  $\epsilon^\infty$ . Knowledge of these quantities is also important to study ferroelectric materials, in which a phase transition takes place due to the interplay between long-range Coulomb interactions and short-range forces [56]. The calculated  $\epsilon^\infty$  and the diagonal elements of  $Z^*$  are reported in Table II for both phases, where they are compared to the available experimental data. The calculated values of  $Z^*$  are observed to be in good agreement with previous DFT calculations [59–61].

We observe that the values of some elements of  $Z^*$  (Ti and O) deviate significantly from their nominal ionic charges. This behavior is in line with that exhibited by other perovskite oxides [60–62] but opposite to that of fluoroperovskites [11]. These strongly anomalous  $Z^*$  play an important role in explaining the emergence of ferroelectricity in perovskite oxides [63].

When comparing  $Z^*$  for both phases at 0 K, we find that  $Z^*(\text{Ba})$  remains almost unchanged, and there is a slight change of about 3% in  $Z^*(\text{Ti})$  along the  $x$  and  $y$  directions, but a significant change of about 21% is observed along the  $z$  axis. In the tetragonal phase there are two inequivalent oxygen atoms:  $Z^*(\text{O}2)$  remains almost the same as in the cubic structure, but for  $Z^*(\text{O}1)$  a decrease by 20% for the  $z$  direction compared to the cubic values can be seen. In addition, the  $x$  and  $y$  directions become slightly different due to the rotation of the O octahedra. We also observe that at the thermalized volume (as a result  $Z^*$  indirectly depends on temperature) the value of  $Z^*$  decreases, but the effect is relatively small, changing mostly in the second digit after the decimal.

TABLE II. Born effective charge tensor  $Z^*$  of Ba, Ti, and O and the dielectric tensor  $\epsilon^\infty$  calculated with the PBEsol functional for both cubic and tetragonal phases. Only the diagonal elements of  $Z^*$  (in the order  $Z_{xx}^*$ ,  $Z_{yy}^*$ ,  $Z_{zz}^*$ ) are shown. For the elements of the dielectric tensor, values in parentheses represent experimental data.

	Nominal	Cubic	Tetragonal
$Z^*(\text{Ba})$	+2	2.77	2.76
	+2	2.77	2.76
	+2	2.77	2.85
$Z^*(\text{Ti})$	+4	7.26	6.98
	+4	7.26	6.98
	+4	7.26	5.98
$Z^*(\text{O}1)$	−2	−2.14	−2.04
	−2	−2.14	−2.04
	−2	−5.76	−4.59
$Z^*(\text{O}2)$	−2		−1.97
	−2		−2.14
	−2		−5.59
$\epsilon_{xx}^\infty$		6.00 (5.40) [57]	5.74 (5.93) [58]
$\epsilon_{zz}^\infty$			5.38 (5.60) [58]

Due to the symmetry of the ferroelectric tetragonal phase, the dielectric tensor  $\epsilon^\infty$  is diagonal but has different values for parallel and perpendicular directions to the  $z$  axis. Our calculated  $\epsilon^\infty$  components are comparable in magnitude to experiment, but the experimental values of  $\epsilon^\infty$  increase from the cubic to the tetragonal structure, while our calculated values show the opposite behavior. Like for  $Z^*$ , there is a negligible effect of volume on  $\epsilon^\infty$ .

### C. Phonon spectrum

The calculated phonon spectra and density of states (DOS) of cubic and tetragonal BaTiO<sub>3</sub> are shown in Figs. 2 and 3, respectively. With five atoms in the unit cell, the cubic perovskites have 15 phonon modes in total. Neglecting the transverse and longitudinal optical (LO–TO) splitting, there are five triply degenerate modes at the  $\Gamma$  point, out of which, four have the irreducible representation  $T_{1u}$  and one has  $T_{2u}$ .

The left panel of Fig. 2 shows the phonon dispersion relations for cubic BaTiO<sub>3</sub> where the splitting of LO–TO phonon modes at the  $\Gamma$  point is included using the Born effective charges  $Z^*$  and the method proposed by Gonze *et al.* [70] as implemented in the PHONOPY code [32]. Gray lines show the phonon spectra calculated using nonthermalized displacements. It is clear that the cubic phase is unstable and that unstable phonons are present in large parts of the Brillouin zone with a maximum instability at the  $\Gamma$  point. The phonon at the mode  $\Gamma$  point is the ferroelectric soft mode responsible for the cubic-to-tetragonal phase transition. Using the SCP approach, all of these imaginary modes are stabilized at elevated temperatures, as shown by the blue lines. For comparisons, phonon frequencies from different experimental studies are also shown. Phonon spectra calculated using both thermalized displacements and volume at 500 K reproduce the experimental frequencies very well. There are some exceptions along  $\Gamma$ -X where the experimental frequencies (shown by triangles



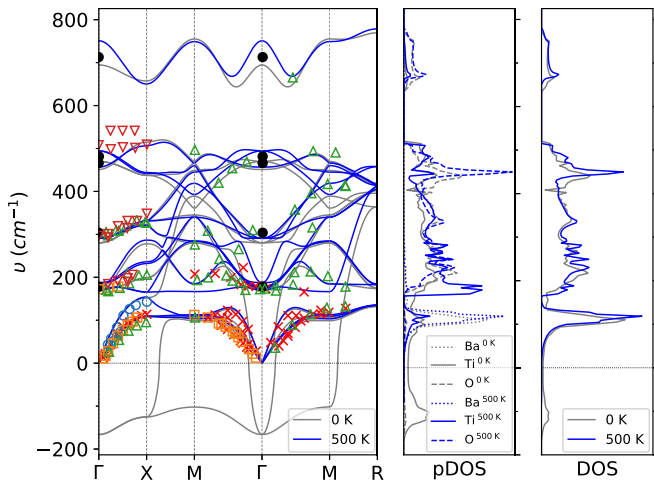


FIG. 2. Phonon band structure along a high-symmetry path and partial and total phonon DOSs in the cubic phase. Gray lines are obtained with nonthermalized displacements at 0 K equilibrium volume, and blue lines are obtained with thermalized displacements at volume corresponding to 500 K. The partial Ba DOS is scaled down by a factor of 4. Experimental data:  $\bullet$ , Ref. [64];  $\times$ , Ref. [65];  $\nabla$ , Ref. [66];  $\triangle$ , Ref. [67];  $\square$ , Ref. [68];  $\circ$ , Ref. [69].

around  $500 \text{ cm}^{-1}$ ) are underestimated by our calculations. Obviously, the unstable phonon modes are most susceptible to temperature effects, and the  $T_{1u}$  frequency at  $\Gamma$  jumps from  $166i$  to  $170 \text{ cm}^{-1}$ .

Figure 3 shows the phonon spectra for both the HA (gray lines) and the SCP approach at 400 K (blue lines) for the tetragonal phase. In terms of the irreducible representations of point group  $4mm$  ( $C_{4v}$ ) the phonon modes at the  $\Gamma$  point in the ferroelectric tetragonal phase can be decomposed into  $4A_1 \oplus B_1 \oplus 5E$ . The macroscopic electric field is responsible for the LO–TO splitting in the infrared-active modes. Due to symmetry, this splitting occurs in different  $\mathbf{q}$  directions in

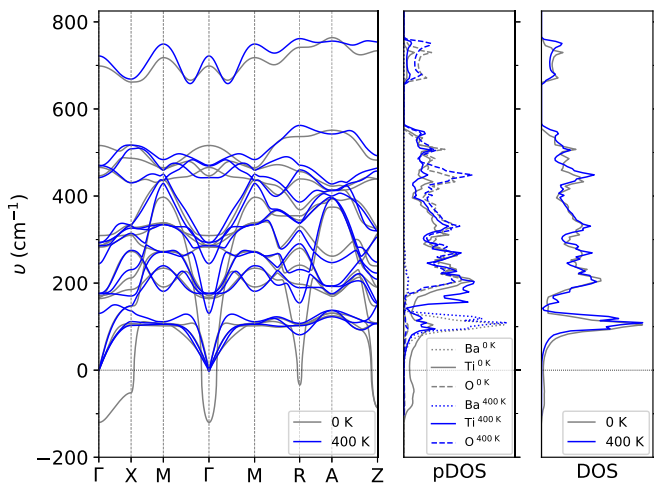


FIG. 3. Phonon band structure along a high-symmetry path and partial and total phonon DOSs of  $\text{BaTiO}_3$  in the tetragonal phase as obtained from nonthermalized and thermalized displacements at 0 K (gray) and 400 K (blue), respectively. Note that the partial Ba DOS is scaled down by a factor of 4.

TABLE III. Calculated and experimental frequencies (in  $\text{cm}^{-1}$ ) of the TO and LO phonon modes of the tetragonal phase of  $\text{BaTiO}_3$  at the  $\Gamma$  point.  $V_{0\text{K}}$  and  $V_{400\text{K}}$  represent the volume calculated at 0 and 400 K, respectively.

		Calculated			Experiment	
		0 K ( $V_{0\text{K}}$ )	400 K ( $V_{0\text{K}}$ )	400 K ( $V_{400\text{K}}$ )		400 K [71]
$A_1$	TO1	164	178	176	178	
	LO1	183	180	180	189	
	TO2	309	333	245	276	
	LO2	456	447	456	471	
	TO3	516	461	469	515	
	LO3	724	706	655	725	
	$E$	TO1	$120i$	141	130	38
		LO1	171	175	176	180
TO2		171	176	176	180	
LO2		286	294	292	308	
	TO3	287	295	294	308	
	LO3	446	454	442	466	
	TO4	466	488	470	498	
	LO4	698	732	722	722	
$B$		283	290	286	304	

reciprocal space for different modes. Two of the  $A_1$  modes acquire different frequencies according to whether the wave vector  $\mathbf{q}$  is orthogonal or parallel to the  $c$  axis (TO and LO modes, respectively). The  $E$  modes are split into  $E(\text{TO})$  and  $E(\text{LO})$  for  $\mathbf{q}$  vectors orthogonal to the  $c$  axis, whereas they do not show any LO–TO splitting for  $\mathbf{q}$  vectors parallel to the  $c$  axis.

Table III illustrates the effect of nonanalytical corrections to the phonon frequencies for tetragonal  $\text{BaTiO}_3$ , and experimental results are also given for comparison [71]. Frequencies calculated at 400 K with the volume obtained at 0 and 400 K are written in the third and fourth columns, respectively, while the fifth column presents experimental frequencies at 400 K. We observe that changing temperature and changing volume have opposite effects on most phonon modes at constant volume and temperature, respectively. In most cases, an increase in temperature hardens the phonon frequencies except for some  $A_1$  optical modes. Thermal expansion also has a sizable effect on the phonon spectra, and in most of the cases phonon frequencies soften with increasing volume. The SCP approach correctly stabilizes the tetragonal structure, giving phonon frequencies in good agreement with experiments. The soft  $E(\text{TO1})$  mode, which exhibits a pronounced temperature dependence as anticipated, acquires a much larger value ( $130 \text{ cm}^{-1}$ ) than that found in experiment ( $38 \text{ cm}^{-1}$ ). The strong temperature dependence of this frequency means that the computed result is highly dependent on small changes in unit-cell volume (DFT approximation) and the chosen probability distribution function.

The middle and right panels of Figs. 2 and 3 show the calculated partial and total phonon DOSs at 0 K and finite temperature with thermalized displacements and volume of the cubic and tetragonal phases, respectively. In the cubic phase at 0 K the DOS corresponding to imaginary frequencies is predominantly due to the Ti atom. The acoustic modes

produce a dominating peak in the frequency range from 80 to 120  $\text{cm}^{-1}$ , and the partial DOS indicates that these modes can be mainly attributed to vibrations of Ba atoms, which is expected due to the heavy mass of Ba. The Ti and O atoms contribute evenly in the frequency range of 150 to 500  $\text{cm}^{-1}$ . Finally, a single mode originating mainly from the vibrations of the O atoms contributes to the DOS at the highest frequency values (660  $\text{cm}^{-1}$  and above). Overall, the shapes of the DOS at 0 and 500 K are quite similar except that the Ti partial DOS at imaginary frequencies is shifted to 145–185  $\text{cm}^{-1}$ , the narrow Ba peak has a slight shift to higher frequencies due to the larger volume at 500 K, and the O partial DOS peak around 450  $\text{cm}^{-1}$  is further increased.

The total and partial phonon DOSs of the tetragonal phase are qualitatively quite similar to the cubic one. Also the temperature effects are pretty much the same and do not need to be repeated here explicitly.

#### D. Thermodynamics of the phase transition

We have studied the critical temperature for the tetragonal-to-cubic phase transition by means of *ab initio* thermodynamics calculations.

At the thermodynamic equilibrium, for fixed pressure  $P$  and temperature  $T$ , the Gibbs free energy,  $G(P, V) = U - TS + PV$ , is at a minimum, where  $U$  and  $S$  represent the internal energy and entropy of the system, respectively. For solids at ambient conditions, the Gibbs free energy is generally well approximated by the Helmholtz free energy  $F = U - TS$ . For insulators, using the adiabatic approximation,  $F$  can be decomposed into electronic and vibrational parts as

$$F(T, V) = E_{\text{elec}}(V) + F_{\text{vib}}(T, V) \\ = E_{\text{elec}}(V) + U_{\text{vib}}(T, V) - TS_{\text{vib}}(T, V), \quad (4)$$

where  $E_{\text{elec}}$  represents the electronic (static) energy, calculated by first-principles, and  $F_{\text{vib}}$  is the vibrational free energy calculated with the SCP approach. The vibrational internal energy and entropy are given by

$$U_{\text{vib}} = \sum_{qs} \left( \langle n(\mathbf{q}s) \rangle + \frac{1}{2} \right) \hbar\omega(\mathbf{q}s), \quad (5)$$

$$S_{\text{vib}} = \sum_{qs} \left[ \frac{\langle n(\mathbf{q}s) \rangle}{T} \hbar\omega(\mathbf{q}s) - k_B T \ln(1 - e^{\hbar\omega(\mathbf{q}s)/k_B T}) \right]. \quad (6)$$

As our model includes anharmonic effects into an effective harmonic Hamiltonian by sampling from the Gaussian distribution of Eq. (3), the formulas derived by considering independent phonons are still valid within our approach. In calculating  $F_{\text{vib}}$ , we also took into account the nonanalytic correction to the dynamical matrix. The comparison between  $U_{\text{vib}}$  and  $S_{\text{vib}}$  times the temperature  $T$  for both phases is shown in Fig. 4. It is clear that both terms cross around  $\approx 420$  K for both phases. Below 420 K, the vibrational internal energy  $U_{\text{vib}}$  dominates, while above 420 K, the vibrational entropy contribution  $TS_{\text{vib}}$  takes over. As a result, the vibrational free energy  $F_{\text{vib}}$  changes sign around 420 K, which means that the value of  $F_{\text{vib}}$  is positive below 420 K and negative above 420 K. Figure 4 also shows that as the temperature increases, the vibrational entropy of the cubic phase becomes larger than for the tetragonal phase while the vibrational internal

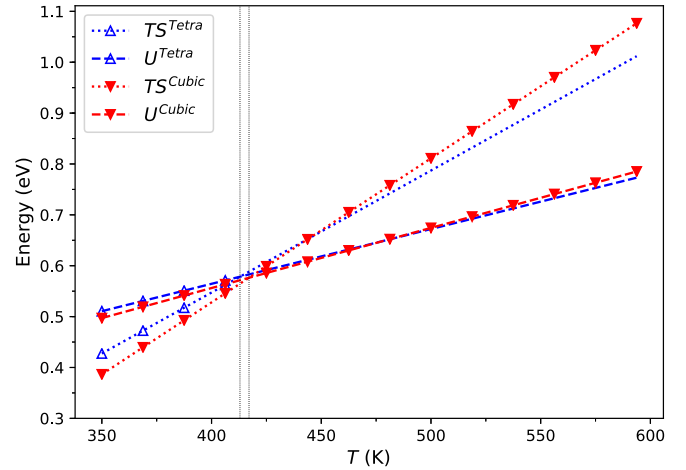


FIG. 4. The vibrational internal energy  $U$  (dashed lines) is shown in comparison to the vibrational entropy  $S$  times temperature  $T$  (dotted lines) for cubic (red) and tetragonal (blue) structures. The vertical black lines represent the crossing point between  $U$  and  $TS$ .

energies remain quite similar. Therefore, the cubic structure is stabilized at high temperature by the vibrational entropy.

We can assess the ferroelectric phase transition by evaluating the difference in the Helmholtz free energy between the two phases,

$$\Delta F(T) = F^{\text{Tetra}}(T) - F^{\text{Cubic}}(T). \quad (7)$$

This quantity is shown in Fig. 5. For both phases, we took into account the change in the volume due to thermal expansion. We found that inclusion of thermal expansion plays an important part in the prediction of the  $T_c$ . Ignoring thermal expansion, the value of the predicted  $T_c$  would be some 40 K higher.

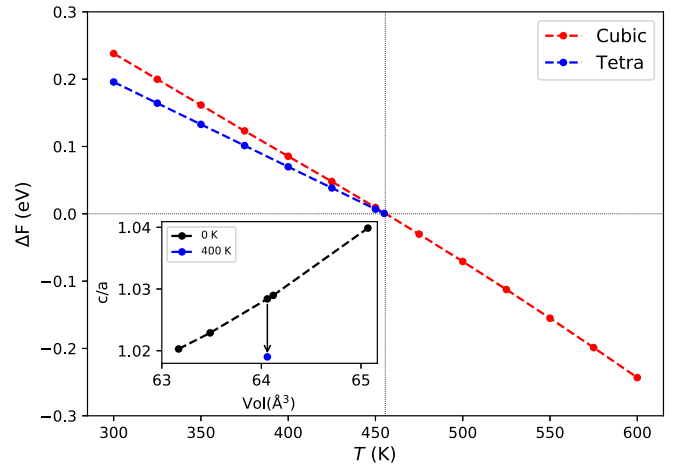


FIG. 5. Calculated free energies of both cubic and tetragonal  $\text{BaTiO}_3$  as a function of temperature. The free energy of the two structures at the phase transition sets the zero in the energy scale. The vertical black line represents the temperature where the (predicted) phase transition occurs, whereas  $\bullet$  show the exact data points. The inset illustrates the volume dependence of the  $c/a$  ratio in the tetragonal phase at 0 K (black) and the change in  $c/a$  at 64.06  $\text{\AA}^3$  with the change in temperature from 0 to 400 K (blue).

Along with the thermal expansion, the change in sign of  $F_{\text{vib}}$  around 420 K is also significant. Due to the opposite sign, the effect of  $F_{\text{vib}}$  is not minimized but, in fact, further enhanced during the evaluation of Helmholtz free energy. By calculating the electronic energy difference ( $\Delta E_{\text{elec}} = 14.28$  meV) of both phases, we observe that  $\Delta E_{\text{elec}}$  has a smaller effect in predicting  $T_c$  compared to the vibrational free energy. Nevertheless,  $\Delta E_{\text{elec}}$  is important because it makes a difference of around 10 K in  $T_c$ . As a result, the predicted phase temperature  $T_c \approx 455$  K is not far off from the experimental value of 393 K. The residual difference in value between calculated and experimental transition temperatures may be due to the specific choice of the exchange-correlation energy functional and the approximate nature of our approach.

The inset in Fig. 5 shows the dependence of  $c/a$  on volume at 0 K (black) and 400 K (blue). Optimization of  $c/a$  at 400 K was done with the help of the SCP method. We start with a two-dimensional grid of  $c/a$  and volume and calculate the vibrational free energy with the SCP approach. Adding these values to the corresponding electronic energy gives the desired free energy. A parabolic fit of  $c/a$  versus free energy gives the minimum value of the free energy vs  $c/a$  at 400 K. We found that temperature plays an important role in determining  $c/a$ . If we include only the volume expansion ( $63.57 \rightarrow 64.06 \text{ \AA}^3$ ), then  $c/a$  increases from 1.022 to 1.0284 at 0 K. However, after the inclusion of both temperature and volume effects, the value of  $c/a$  decreases from 1.0284 to 1.0190, which is in the right direction. The  $c/a$  value is still overestimated, which is due to the fact that the starting  $c/a$  at 0 K is too large and the effects of temperature are not big enough to neutralize the effect of the large  $c/a$  increase with volume at 0 K.

## V. DISCUSSIONS AND SUMMARY

It is worthwhile to compare our results on  $\text{BaTiO}_3$  with those of Monte Carlo simulations based on the effective Hamiltonian as presented in Refs. [61,72] and discussed, e.g., in Ref. [63]. Combining the symmetry analysis of the underlying Landau theory with the induced representations of site symmetry groups [73], one constructs a microscopic Hamiltonian from a localized [74] soft phonon mode driving the transition coupled to strain, with all coupling parameters calculated from DFT. The resulting effective Hamiltonian is then “heated up” by feeding it to Metropolis Monte Carlo simulations. Yet the numerical predictions of the corresponding  $T_c$  were off by almost 100 K from experiment [61,72]. The main source of the discrepancy was identified as the inherent neglect of couplings to “noncritical” modes in setting up the effective Hamiltonian, which results in a poor description of thermal expansion [75]. Tweaking the simulations “by hand” in order to force the effective Hamiltonian to follow a reasonable thermal expansion behavior, the resulting error in  $T_c$  could be reduced to 5%.

Based on our present method, we observe that ignoring thermal expansion in our SCP approach shifts  $T_c$  in the op-

posite direction and a further increase (and thus a worsening) of our prediction for  $T_c$ . In a certain way, the QHA-SCP approach, in which the noncritical effects of thermal expansion are taken well into account while the critical anharmonicity related to the soft mode is treated in a SCP approximation, may be seen as complementary to the effective Hamiltonian method, in which emphasis was put on a precise treatment of the soft mode while noncritical phonon effects are largely ignored. An important lesson to be learned from this comparison is that a proper description of thermal expansion seems to be mandatory for a concise prediction of  $T_c$ .

The importance of thermal expansion can also be seen by comparing our results to earlier studies. The SCP study of phase transitions in perovskites has mainly been aimed at the phonon band structure at finite temperature [19], but this may not be a good proxy for  $T_c$ . The studies of  $\text{SnSe}$ , which exhibits a phase transition from primitive to centered orthorhombic at approximately 800 K, are interesting in this context. Imaginary frequencies in the phonon driving the phase transition have been found to disappear at temperatures between 180 K (LDA) and 300 K (PBE) far below the phase transition [76]. In contrast, a  $T_c$  of approximately 1200 K for the transition was found using free energies in an approach similar to the present one [77]. This overestimation can be mainly attributed to an overestimated equilibrium volume inherent in the PBE functional, and applying a pressure of 4 GPa resulted in a calculated  $T_c$  of 800 K [77]. These examples emphasize the importance of a proper description of volume expansion and the influence of a particular DFT approximation. We also mention the work of Tadano and Tsuneyuki [18] on  $\text{SrTiO}_3$ . Using effective IFCs from *ab initio* molecular dynamics and random displacements, the study included fourth-order force constants but neglected unit-cell changes and obtained a  $T_c$  of 80 K compared to the experimental  $T_c = 105$  K.

Obviously, any effective harmonic model must be an approximation, but the present results demonstrate the power of this approach. In particular, when soft phonons depend so critically on volume and the  $c/a$  ratio, the underlying DFT approximation may produce the largest error in the theoretical modeling. This is best illustrated in  $\text{BaTiO}_3$  by the large changes in the  $T = 0$  equilibrium volume and  $c/a$  ratio using various DFT approximations [48]. Also, the  $\Gamma$  point phonon instability nearly doubles from  $140i$  to  $240i \text{ cm}^{-1}$  when changing from LDA to PBE. We also consider the limited accuracy of our predicted volume, and the  $c/a$  ratio changes as a function of temperature mainly as a DFT problem.

In summary we have calculated structural and vibrational properties of  $\text{BaTiO}_3$  in its cubic and tetragonal phases at 0 K and finite temperatures. By following the SCP approach, we have obtained phonon spectra of the cubic and tetragonal phases at finite temperatures, obtaining phonon frequencies which are stable within the whole Brillouin zone. The calculated frequencies are also in very good agreement with available experimental data at given temperatures. Last, by calculating free energies we have predicted  $T_c \approx 455$  K, which is in reasonable agreement with the experimental value of 393 K.

## ACKNOWLEDGMENTS

P.B. and S.E. acknowledge support from the Austrian Science Fund (FWF) Project No. P27738-N28. A.T. acknowledges support from the Austrian Science Fund (FWF) Project

No. P27738-N28. G.K.H.M. acknowledges support from the Austrian Science Fund (FWF) Project CODIS (I 3576-N36). S.E. acknowledges support from the Higher Education Commission of Pakistan.

- [1] C. J. Howard and H. T. Stokes, *Acta Crystallogr., Sect. A* **61**, 93 (2005).
- [2] P. S. Whitfield, N. Herron, W. E. Guise, K. Page, Y. Q. Cheng, I. Milas, and M. K. Crawford, *Sci. Rep.* **6**, 35685 (2016).
- [3] H. Thomas and K. A. Müller, *Phys. Rev. Lett.* **21**, 1256 (1968).
- [4] C. N. W. Darlington, *Phys. Status Solidi B* **76**, 231 (1976).
- [5] C. Lu, M. Wu, L. Lin, and J.-M. Liu, *Natl. Sci. Rev.* **6**, 653 (2019).
- [6] L. Qiao, S. Zhang, H. Y. Xiao, D. J. Singh, K. H. L. Zhang, Z. J. Liu, X. T. Zu, and S. Li, *J. Mater. Chem. C* **6**, 1239 (2018).
- [7] Y. Bai, T. Siponkoski, J. Peräntie, H. Jantunen, and J. Juuti, *Appl. Phys. Lett.* **110**, 063903 (2017).
- [8] Y.-M. You, W.-Q. Liao, D. Zhao, H.-Y. Ye, Y. Zhang, Q. Zhou, X. Niu, J. Wang, P.-F. Li, D.-W. Fu, Z. Wang, S. Gao, K. Yang, J.-M. Liu, J. Li, Y. Yan, and R.-G. Xiong, *Science* **357**, 306 (2017).
- [9] A. R. Oganov and S. Ono, *Nature (London)* **430**, 445 (2004).
- [10] E. Blokhin, D. Gryaznov, E. Kotomin, R. Evarestov, and J. Maier, *Integr. Ferroelectr.* **123**, 18 (2011).
- [11] S. Ehsan, A. Tröster, F. Tran, and P. Blaha, *Phys. Rev. Mater.* **2**, 093610 (2018).
- [12] A. Marronnier, H. Lee, B. Geffroy, J. Even, Y. Bonnassieux, and G. Roma, *J. Phys. Chem. Lett.* **8**, 2659 (2017).
- [13] P. Souvatzis, S. Arapan, O. Eriksson, and M. I. Katsnelson, *Europhys. Lett.* **96**, 66006 (2011).
- [14] O. Hellman, I. A. Abrikosov, and S. I. Simak, *Phys. Rev. B* **84**, 180301(R) (2011).
- [15] I. Errea, M. Calandra, and F. Mauri, *Phys. Rev. Lett.* **111**, 177002 (2013).
- [16] T. Tadano and S. Tsuneyuki, *Phys. Rev. B* **92**, 054301 (2015).
- [17] A. van Roekeghem, J. Carrete, C. Oses, S. Curtarolo, and N. Mingo, *Phys. Rev. X* **6**, 041061 (2016).
- [18] T. Tadano and S. Tsuneyuki, *J. Ceram. Soc. Jpn.* **127**, 404 (2019).
- [19] B. Xu, O. Hellman, and L. Bellaiche, *Phys. Rev. B* **100**, 020102(R) (2019).
- [20] S. A. Hayward and E. K. H. Salje, *Phase Transitions* **68**, 501 (1999).
- [21] H. Zhang, S. Liu, M. E. Scofield, S. S. Wong, X. Hong, V. B. Prakapenka, E. Greenberg, and T. A. Tyson, *Appl. Phys. Lett.* **111**, 052904 (2017).
- [22] A. Tröster, S. Ehsan, K. Belbase, P. Blaha, J. Kreisel, and W. Schranz, *Phys. Rev. B* **95**, 064111 (2017).
- [23] A. Tröster, W. Schranz, F. Karsai, and P. Blaha, *Phys. Rev. X* **4**, 031010 (2014).
- [24] T. Xu, T. Shimada, Y. Uratani, X. Wang, J. Wang, and T. Kitamura, *Sci. Rep.* **7**, 45373 (2017).
- [25] Q. Zhang, T. Cagin, and W. A. Goddard, *Proc. Natl. Acad. Sci. USA* **103**, 14695 (2006).
- [26] M. G. Harwood, P. Popper, and D. F. Rushman, *Nature (London)* **160**, 58 (1947).
- [27] B. Ravel, E. A. Stern, R. I. Vedral, and V. Kraizman, *Ferroelectrics* **206**, 407 (1998).
- [28] C. Eiseenschmidt, H. T. Langhammer, R. Steinhausen, and G. Schmidt, *Ferroelectrics* **432**, 103 (2012).
- [29] Y. Bai, K. Ding, G.-P. Zheng, S.-Q. Shi, J.-L. Cao, and L. Qiao, *AIP Adv.* **2**, 022162 (2012).
- [30] O. Hellman, P. Steneteg, I. A. Abrikosov, and S. I. Simak, *Phys. Rev. B* **87**, 104111 (2013).
- [31] M. Born and K. Huang, *Dynamical Theory of Crystal Lattices* (Oxford University Press, Oxford, 1954).
- [32] A. Togo and I. Tanaka, *Scr. Mater.* **108**, 1 (2015).
- [33] D. Alfè, *Comput. Phys. Commun.* **180**, 2622 (2009).
- [34] K. Parlinski, software PHONON, Cracow, Poland (2013).
- [35] P. Souvatzis, O. Eriksson, M. I. Katsnelson, and S. P. Rudin, *Phys. Rev. Lett.* **100**, 095901 (2008).
- [36] R. Stern and G. K. H. Madsen, *Phys. Rev. B* **94**, 144304 (2016).
- [37] R. Stern, T. Wang, J. Carrete, N. Mingo, and G. K. H. Madsen, *Phys. Rev. B* **97**, 195201 (2018).
- [38] B. T. M. Willis and A. W. Pryor, *Thermal Vibrations in Crystallography* (Cambridge University Press, Cambridge, 1975).
- [39] T. Tadano and S. Tsuneyuki, *Nature (London)* **155**, 484 (1945).
- [40] G. Schulze, *Z. Angew. Math. Mech.* **43**, 512 (1963).
- [41] K. Toyoda, *Ferroelectrics* **23**, 209 (1980).
- [42] L. Carlsson, *Acta Crystallogr.* **20**, 459 (1966).
- [43] P. Blaha, K. Schwarz, G. K. H. Madsen, D. Kvasnicka, J. Luitz, R. Laskowski, F. Tran, and L. D. Marks, *WIEN2K: An Augmented Plane Wave plus Local Orbitals Program for Calculating Crystal Properties* (Techn. Universität Wien, Vienna, 2018).
- [44] P. Blaha, K. Schwarz, F. Tran, R. Laskowski, G. K. H. Madsen, and L. D. Marks, *J. Chem. Phys.* **152**, 074101 (2020).
- [45] W. Kohn and L. J. Sham, *Phys. Rev.* **140**, A1133 (1965).
- [46] J. P. Perdew, A. Ruzsinszky, G. I. Csonka, O. A. Vydrov, G. E. Scuseria, L. A. Constantin, X. Zhou, and K. Burke, *Phys. Rev. Lett.* **100**, 136406 (2008).
- [47] J. P. Perdew, K. Burke, and M. Ernzerhof, *Phys. Rev. Lett.* **77**, 3865 (1996).
- [48] R. Wahl, D. Vogtenhuber, and G. Kresse, *Phys. Rev. B* **78**, 104116 (2008).
- [49] A. Tröster, W. Schranz, S. Ehsan, K. Belbase, and P. Blaha, *Crystals* **10**, 124 (2020).
- [50] F. D. Murnaghan, *Proc. Natl. Acad. Sci. USA* **30**, 244 (1944).
- [51] S. F. Yuk, K. C. Pitike, S. M. Nakhmanson, M. Eisenbach, Y. W. Li, and V. R. Cooper, *Sci. Rep.* **7**, 43482 (2017).
- [52] T. Nakatani, A. Yoshiasa, A. Nakatsuka, T. Hiratoko, T. Mashimo, M. Okube, and S. Sasaki, *Acta Crystallogr., Sect. B* **72**, 151 (2016).
- [53] P. Puffer, *Cryst. Res. Technol.* **18**, 1546 (1983).
- [54] G. J. Fischer, Z. Wang, and S.-i. Karato, *Phys. Chem. Miner.* **20**, 97 (1993).
- [55] M. Born, *Math. Proc. Cambridge Philos. Soc.* **36**, 160 (1940).
- [56] P. Ghosez, X. Gonze, and J.-P. Michenaud, *Europhys. Lett.* **33**, 713 (1996).



- [57] G. Burns and F. Dacol, *Solid State Commun.* **42**, 9 (1982).
- [58] M. S. Shumate, *Appl. Opt.* **5**, 327 (1966).
- [59] P. Hermet, M. Veithen, and P. Ghosez, *J. Phys.: Condens. Matter* **21**, 215901 (2009).
- [60] P. Ghosez, J.-P. Michenaud, and X. Gonze, *Phys. Rev. B* **58**, 6224 (1998).
- [61] W. Zhong, R. D. King-Smith, and D. Vanderbilt, *Phys. Rev. Lett.* **72**, 3618 (1994).
- [62] C.-Z. Wang, R. Yu, and H. Krakauer, *Phys. Rev. B* **54**, 11161 (1996).
- [63] K. M. Rabe and P. Ghosez, in *Physics of Ferroelectrics: A Modern Perspective* (Springer, Berlin, 2007), pp. 117–174.
- [64] Y. Luspin, J. L. Servoin, and F. Gervais, *J. Phys. C* **13**, 3761 (1980).
- [65] J. Harada, J. D. Axe, and G. Shirane, *Phys. Rev. B* **4**, 155 (1971).
- [66] J. Bouillot, C. Escribe, W. Fitzgerald, and L. Gnininvi, *Solid State Commun.* **30**, 521 (1979).
- [67] B. Jannot, C. Escribe-Filippini, and J. Bouillot, *J. Phys. C* **17**, 1329 (1984).
- [68] G. Shirane, J. D. Axe, J. Harada, and A. Linz, *Phys. Rev. B* **2**, 3651 (1970).
- [69] G. Shirane, B. C. Frazer, V. J. Minkiewicz, J. A. Leake, and A. Linz, *Phys. Rev. Lett.* **19**, 234 (1967).
- [70] X. Gonze, J.-C. Charlier, D. C. Allan, and M. P. Teter, *Phys. Rev. B* **50**, 13035 (1994).
- [71] A. Scalabrin, A. S. Chaves, D. S. Shim, and S. P. S. Porto, *Phys. Status Solidi B* **79**, 731 (1977).
- [72] W. Zhong, D. Vanderbilt, and K. M. Rabe, *Phys. Rev. B* **52**, 6301 (1995).
- [73] R. A. Evarestov and V. P. Smirnov, *Site Symmetry in Crystals: Theory and Applications*, Springer Series in Solid-State Sciences Vol. 108 (Springer-Verlag, Berlin Heidelberg, 2012).
- [74] K. M. Rabe and U. V. Waghmare, *Phys. Rev. B* **52**, 13236 (1995).
- [75] S. Tinte, J. Íñiguez, K. M. Rabe, and D. Vanderbilt, *Phys. Rev. B* **67**, 064106 (2003).
- [76] U. Aseginolaza, R. Bianco, L. Monacelli, L. Paulatto, M. Calandra, F. Mauri, A. Bergara, and I. Errea, *Phys. Rev. Lett.* **122**, 075901 (2019).
- [77] A. Dewandre, O. Hellman, S. Bhattacharya, A. H. Romero, G. K. H. Madsen, and M. J. Verstraete, *Phys. Rev. Lett.* **117**, 276601 (2016).